

1 Nat. Hazards Earth Syst. Sci., xx, xxx-xxx, 2020
2 [Http://doi.org/](http://doi.org/)
3 © Author(s) 2020. This work is distributed under
4 the Creative Commons Attribution 4.0 License.

5

6

7 **Study on the influence of seafloor soft soil layer on seismic ground**

8 **motion**

9

10 **Jingyan Lan¹, Juan Liu², Xing Song^{1*}**

11 ¹Key Laboratory of Geomechanics and Geotechnical Engineering, Guilin University of
12 Technology, Guilin, Guangxi 541004, China

13 ²Institute of Engineering Mechanics, China Earthquake Administration, Harbin, Heilongjiang
14 150080, China

15 **Correspondence:** Xing Song (425270453@qq.com)

16 **Received:** 12 July 2020 – **Discussion started:** XXXX

17 **Revised:** XXXX – **Accepted:** XXXX – **Published:** XXXX

18

19 **Abstract.** In the complex medium system of sea area, the overlying sea water and the surface
20 soft soil have a significant impact on the seafloor ground motion, which brings great seismic
21 risk to the safety of offshore engineering structures. In this paper, four sets of typical free field
22 models are constructed and established, which are land model, land model with surface soft
23 soil, sea model and sea model with surface soft soil. The dynamic finite difference method is
24 used to carry out two-dimensional seismic response analysis of typical free field based on the
25 input forms about P and SV wave. By comparing the seismic response analysis results of four
26 groups of calculation models, the effects of overlying seawater and soft soil on peak
27 acceleration and acceleration response spectrum are studied. The results show that when SV
28 wave is input, the peak acceleration and response spectrum of the surface of soft soil on the
29 surface and the seabed surface can be amplified, while the overlying sea water can
30 significantly reduce the ground motion. When P wave is used, the effect of overlying seawater
31 and soft soil on peak acceleration and response spectrum of surface and seabed can be ignored.
32 The peak acceleration decreases first and then increases from the bottom to the surface, and
33 the difference of peak acceleration calculated by four free field models is not obvious. The
34 results show that the overlying sea water and the surface soft soil layer have little effect on the
35 peak acceleration of ground motion below the surface.

36 1 Introduction

37 Both empirical and theoretical studies of earthquake damage show that the site conditions,
38 especially the soft soil site conditions, are the important factors that affect the aggravation of
39 surface earthquake damage and the significant amplification of theoretical ground motion
40 (Celebi, 1991; Huang et al., 2009; Kubo et al., 2019; Wang et al., 2019). With the
41 development of offshore engineering in recent years, some of them, such as offshore oil
42 platform, cross sea bridge, subsea tunnel, etc., have been developed rapidly. Therefore,
43 dynamic characteristics of subsea soft soil and its influence on the ground motion are paid
44 more and more attention. The current research mainly focuses on the simulation of land-based
45 ground motion. In the seismic response analysis of the actual sea area engineering site, the
46 influence of the self weight stress of the overlying sea water and the action of the overlying
47 saturated soft soil are ignored (Fan et al., 2018), and the one-dimensional frequency domain
48 or time domain seismic response analysis method consistent with the land area engineering is
49 still used (Idriss and Sun, 1992; Streeter et al., 1974; Bardet et al., 2000; Hashash and Park,
50 2001; Bardet and Tobita, 2001), which is inconsistent with the actual sea area saturated
51 two-dimensional complex medium system. Contemporary studies have shown that the pore
52 water saturation of underwater soil layer has a great influence on the amplitude of vertical
53 in-plane motion (Yang and Sato, 2000; Yang, 2001; Wang and Hao, 2002; Zhang et al., 2012).
54 However, none of these studies considered the effect of the sea water layer on the seismic
55 ground motion in the offshore environment. Boore and Smith (1999) analyzed the seismic
56 records obtained from the undersea seismic survey system deployed off the coast. The
57 theoretical calculation shows that the influence of the sea water layer on the horizontal
58 component of the ground motion can be ignored. Since there are few records of the sea floor
59 movement, some methods have been proposed to simulate the spatial changes of the sea floor
60 movement (Meng, 2007; He et al., 2015). Petukhin et al. (2010) analyzed two real seabed
61 models with and without sea water layer, and concluded that when the thickness of sea water
62 is within 5 km, the effect of sea water layer on Rayleigh wave is significant; when the
63 thickness of sea water is greater than 10 km, the effect of sea water on ground motion can be
64 ignored. Nakamura et al. (2014) used the strong earthquake data recorded on the surface of
65 the Kii Peninsula and near the Nankai Trough to study the abnormal large earthquake
66 amplification in the seabed area. Zhang et al. (2019) deduced the analytical expression of the
67 wave of the seabed foundation site when the P wave or SV wave incident, and thought that the
68 water depth had little influence on the peak value of the horizontal displacement, but the
69 resonance frequency increased with the increase of the thickness of the water layer.

70 In view of this, in order to study the influence of the self weight stress of the overlying sea
71 water, based on the second development of the finite difference software FLAC3D, this paper
72 constructs four typical two-dimensional dynamic calculation models of the free field, carries
73 out two-dimensional seismic response analysis of the free field, systematically studies the
74 influence of the self weight stress of the overlying sea water and the soft soil layer on the peak
75 value and acceleration response spectrum of the ground motion, through comparative analysis
76 The difference of seismic response analysis results of land free field in sea area. The research
77 results are helpful to reveal the influence mechanism of the saturated soil site on the ground
78 motion, and further deepen and enrich the research progress and achievements in this field. In

79 view of this, in order to study the influence of the self weight stress of the overlying sea water,
80 based on the second development of the finite difference software FLAC3D, this paper
81 constructs four typical two-dimensional dynamic calculation models of the free field, carries
82 out two-dimensional seismic response analysis of the free field, systematically studies the
83 influence of the self weight stress of the overlying sea water and the soft soil layer on the peak
84 value and acceleration response spectrum of the ground motion, through comparative analysis
85 The difference of seismic response analysis results of land free field in sea area. The research
86 results are helpful to reveal the influence mechanism of the saturated soil site on the ground
87 motion, and further deepen and enrich the research progress and achievements in this field.

88 2 Brief introduction of seismic response method based on finite difference method

89 The quadrilateral element is utilized to divide the dynamic calculation area, the Mohr
90 Coulomb criterion is used for the nonlinear constitutive model of soil, the free boundary is
91 used for the artificial boundary, and the Rayleigh damping is selected for the damping. The
92 dynamic equation (1), (2) are formed according to the node equilibrium condition. After the
93 earthquake load is input, the fast Lagrangian finite difference method is used to solve the
94 equation. The node velocity (3), (4) and node displacement (5), (6) are obtained, and then the
95 next node is calculated. The above process is reiterated until the end of calculation.

$$96 \quad M_i \ddot{u}_i^t + C_i \dot{u}_i^t + K_i u_i^t = F_{ix}(t) \quad (1)$$

$$97 \quad M_i \ddot{v}_i^t + C_i \dot{v}_i^t + K_i v_i^t = F_{iy}(t) \quad (2)$$

98 Where: M is the mass matrix, C is the damping matrix, K is the stiffness matrix, u_i 、

99 v_i is the node displacement, \dot{u}_i^t 、 \dot{v}_i^t is the node speed, \ddot{u}_i^t 、 \ddot{v}_i^t is the node acceleration, $F_i(t)$

100 is the external force on the node.

$$101 \quad \dot{u}_i^t(t + \frac{\Delta t}{2}) = \dot{u}_i^t(t - \frac{\Delta t}{2}) + \frac{\Delta t}{M} F_{ix} \quad (3)$$

$$102 \quad \dot{v}_i^t(t + \frac{\Delta t}{2}) = \dot{v}_i^t(t - \frac{\Delta t}{2}) + \frac{\Delta t}{M} F_{iy} \quad (4)$$

$$103 \quad u_i(t + \Delta t) = u_i(t) + \Delta t \dot{u}_i(t + \frac{\Delta t}{2}) \quad (5)$$

$$104 \quad v_i(t + \Delta t) = v_i(t) + \Delta t \dot{v}_i(t + \frac{\Delta t}{2}) \quad (6)$$

105 3 Dynamic calculation model

106 Four groups of free field calculation models are designed and constructed, including land
107 layered site model, land layered site model with surface soft soil, sea layered site model and
108 sea layered site model with surface soft soil. The layer thickness and sea water depth of each
109 group of calculation models are presented in Figure 1. In order to effectively analyze the

110 influence of overlying sea water and soft soil layer on ground motion, the layered soil in the
 111 four calculation models in this paper refers to the calculation model of Chen (2016), and in
 112 order to simplify the calculation model and improve the simulation accuracy and efficiency,
 113 this paper regards sea water as ideal fluid and ignores its viscosity, and realizes the influence
 114 of overlying sea water self weight stress by setting dynamic water pressure, The horizontal
 115 layered free field of seawater saturated seabed basement is established. Layered soil in the
 116 four groups of calculation models uses the same physical and mechanical property parameters
 117 (Lan et al., 2012), and the calculation results are shown in Table 1 by using formulas (7) to
 118 (9).
 119

$$G = V_s^2 \rho \quad (7)$$

$$V_p = \sqrt{\frac{\lambda + 2G + \alpha^2 M}{\rho}} = \sqrt{\frac{G(2 - 2\mu') / (1 - 2\mu') + \alpha^2 M}{\rho}} \quad (8)$$

$$K = V_p^2 \rho + \frac{4}{3} G \quad (9)$$

122 Where, G is the shear modulus, V_p is the compression wave velocity, K is the bulk modulus,
 123 μ' is the Poisson's ratio of soil skeleton, α is the compression parameter of soil, and M is the
 124 compression parameter of water.
 125

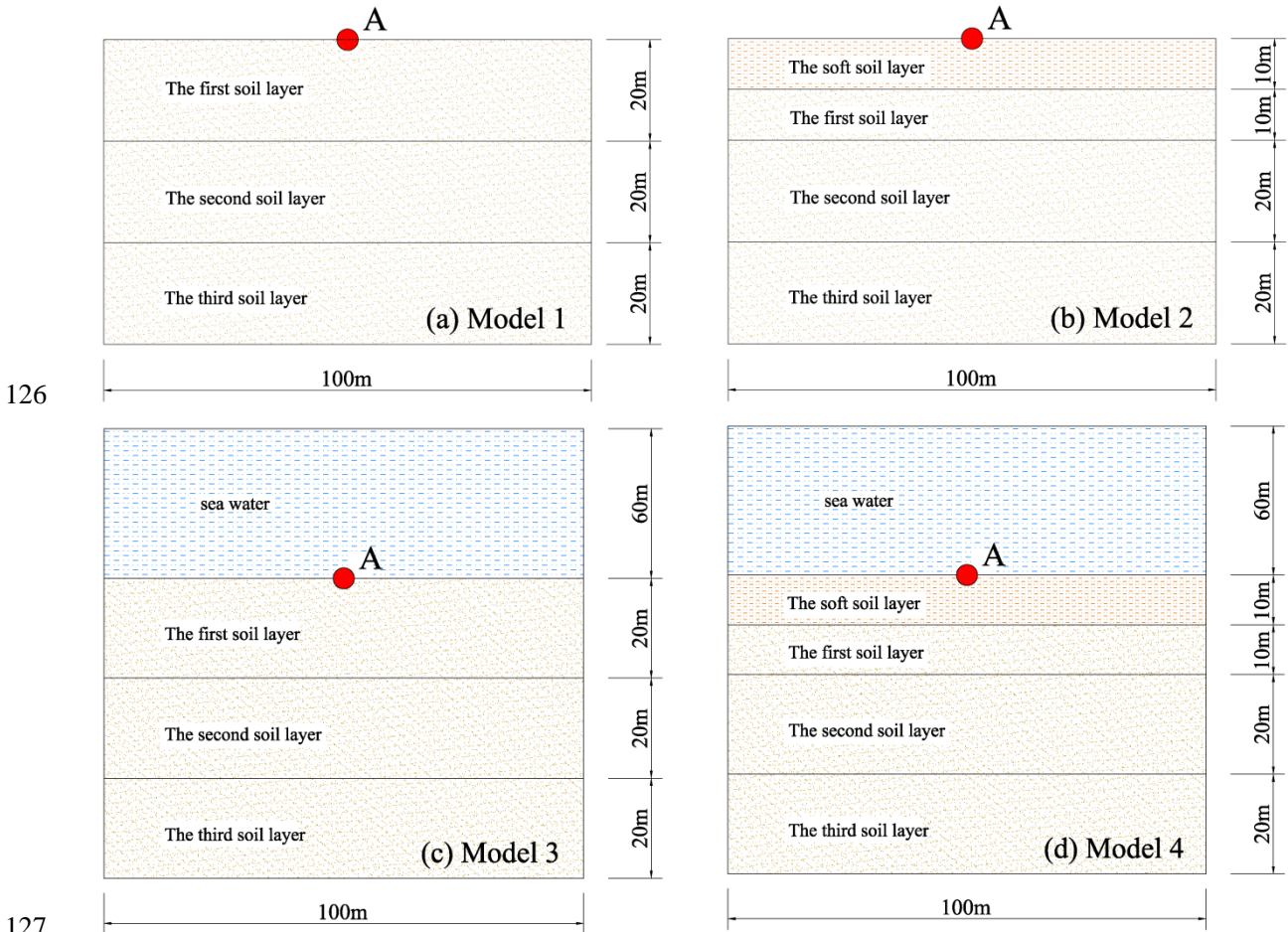


Figure 1. Four typical free field models

130

Table 1. Parameter of stratified layer model

Basic properties	Soft soil layer	First soil layer	Second soil layer	Third soil layer
ρ (kg/m ³)	1500	1700	2000	2250
G (MPa)	48.6	97	221	951
K (MPa)	354	478	6130	9130
v_s (m/s)	180	240	360	650
v_p (m/s)	1550	1700	1800	2170
C (kPa)	10	10	10	6500
φ (°)	18	30	30	45
μ'	0.5	0.5	0.5	0.5

131 Four groups of free field calculation models (Figure 1) are meshed by FLAC3D. According
 132 to the principle that the size of the grid element should not be greater than 1/10 of the
 133 minimum wavelength in the input seismic wave, the wave propagation in the soil layer can be
 134 more accurately simulated, i.e

$$135 \quad \Delta l \leq \left(\frac{1}{10} \sim \frac{1}{8}\right)\lambda \quad (10)$$

$$136 \quad \lambda = \frac{V}{f} \quad (11)$$

137 Where, Δl is the maximum grid size, λ is the minimum input wavelength, f is the highest
 138 frequency of seismic wave, V is the wave velocity of seismic wave.

139 By substituting the soil parameters into the above formula, we can get the value of $\Delta l=3\text{m}$
 140 in the form of SV wave input and $\Delta l=17\text{m}$ in the form of P wave input. In order to improve
 141 the simulation accuracy, the mesh size of SV wave input is $2\text{m}\times 2\text{m}$, and that of P wave input
 142 is $5\text{m}\times 5\text{m}$.

143 4 Analysis of numerical simulation results of earthquake response

144 4.1 Base input ground motion

145 Two representative natural ground motion time history, El Centro wave and Kobe wave, are
 146 selected for the input seismic wave of basement. In order to enhance the calculation efficiency,
 147 the time window of the input base time history is reduced, the first 20s of the time history
 148 curve is intercepted and retained, and the amplitude is scaled at the same time. The two peak
 149 values of seismic wave input are adjusted to 0.20g, which can simulate the seismic response
 150 under the action of a medium strong earthquake. The acceleration time history curve and the
 151 Fourier spectrum of El Centro wave and Kobe wave adjusted by the peak value and duration
 152 is given in Figure 2.

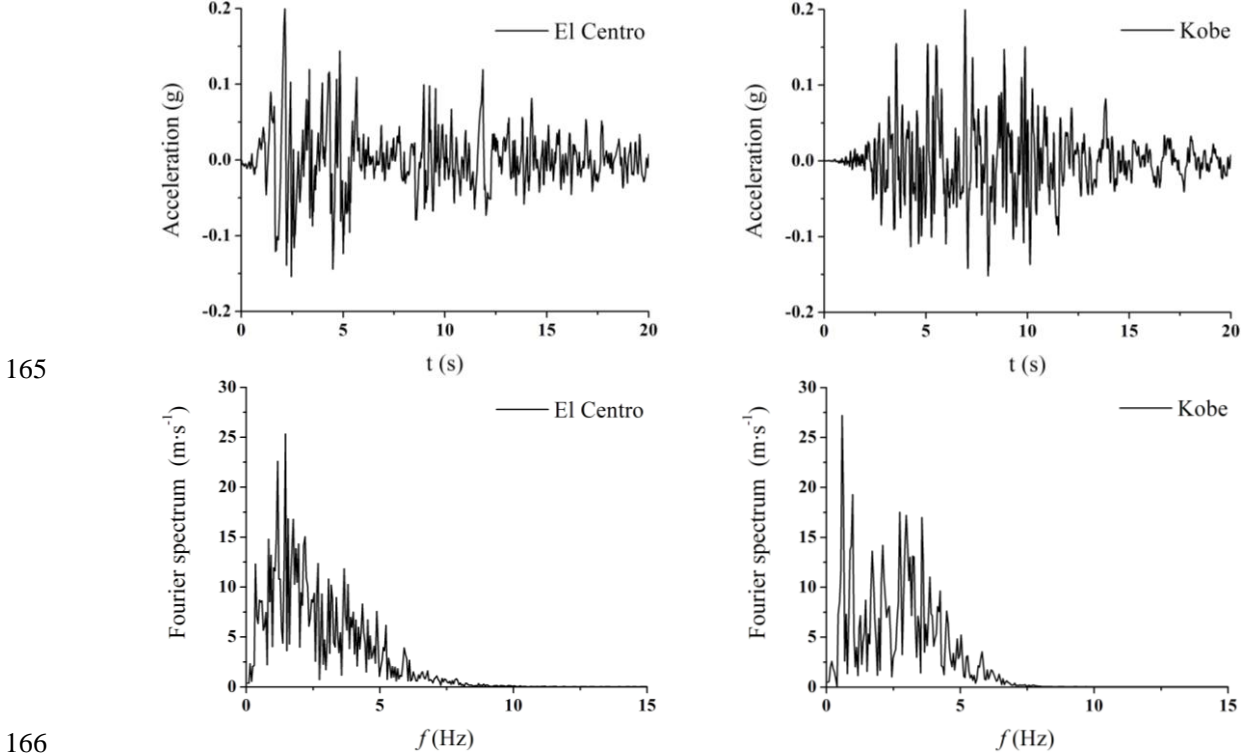
153 4.2 Effect of overlying seawater and soft soil on peak acceleration and amplification 154 coefficient

155 Taking El Centro wave and Kobe wave as the basic input, SV wave and P wave are used
 156 respectively, and the finite difference method introduced in Section 1 is used to carry out the
 157 numerical simulation of two-dimensional free field seismic response analysis. The peak
 158 acceleration of ground motion at a point A of the surface and seabed surface of four groups of

159 free field models is calculated. At the same time, we define a peak amplification coefficient β ,
 160 which is expressed as the ratio of the surface peak acceleration PGA_{surface} to the base input
 161 peak acceleration of PGA_{bedrock} , i.e:

$$162 \quad \beta = \frac{PGA_{\text{surface}}}{PGA_{\text{bedrock}}} \quad (12)$$

163 Then, we get the peak acceleration and peak amplification coefficient of point a, as
 164 showed in Table 2 and Table 3.



165

166

167

168

169

Figure 2. Acceleration time history curve of seismic waves

Table 2. Surface peak acceleration PGA_{surface} of monitoring point A

Base input	Input form	Model 1	Model 2	Model 3	Model 4
El Centro	SV	0.659	0.774	0.651	0.705
	P	0.119	0.120	0.128	0.130
Kobe	SV	0.421	0.534	0.393	0.509
	P	0.119	0.120	0.123	0.123

170

Table.3 Peak amplification coefficient β of monitoring point A

Base input	Input form	Model 1	Model 2	Model 3	Model 4
El Centro	SV	3.29	3.87	3.26	3.57
	P	0.59	0.60	0.64	0.65
Kobe	SV	2.10	2.67	1.97	2.55
	P	0.59	0.60	0.61	0.62

171 It can be seen from the above results that when the seismic wave is input at the base in the
 172 form of SV wave, the peak acceleration and amplification coefficient β of point a of the four
 173 calculation models are obviously different. The results with the largest peak value and
 174 amplification coefficient are the land model with surface soft soil, then the sea model with
 175 surface soft soil, then the land model, and the sea model with the smallest result. Therefore, it

176 can be concluded that the surface soft soil can amplify the peak acceleration of the surface
 177 and the seabed surface, while the overlying sea water can significantly reduce the ground
 178 motion. It can also be seen from the results in Table 2 and table 3 that under the same set of
 179 calculation model conditions, the calculation results for El Centro wave as the basic input is
 180 higher than those with Kobe wave input

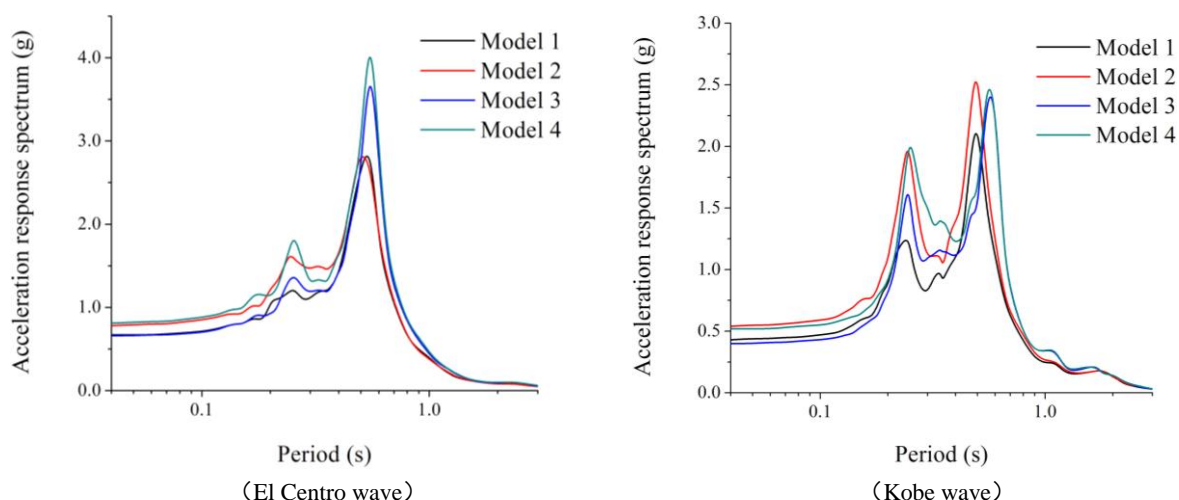
181 When the seismic wave is input as a base in the form of P-wave, the peak acceleration and
 182 amplification coefficient β of point a of the four calculation models are almost the same. The
 183 main reason for this phenomenon may be that the overlying sea water and the self weight of
 184 the soil layer restrain the seismic response and amplification effect of P wave as vertical input.
 185 At the same time, because of the property of P wave and the direction of vibration
 186 propagation, the vertical seismic action of P wave is small. However, the SV wave is
 187 horizontal input and perpendicular to the propagation direction, which can cause soil shear
 188 deformation. Furthermore, it can also be shown that in the seismic design and time history
 189 analysis of practical projects, the shear effect of horizontal ground motion is still the primary
 190 consideration and attention.

191 4.3 Effect of overlying seawater and soft soil on acceleration response spectrum

192 After calculation and analysis, the acceleration response spectra of four groups of free field
 193 models at point A of the surface and seabed surface under the input of El Centro wave and
 194 Kobe wave in the form of P and SV wave are given, as shown in Figure 3 and Figure 4.

195 It can be seen from Figure 3 that when El Centro wave is input in the form of SV wave,
 196 the acceleration response spectrum reaches the maximum value when the period is 0.6s, and
 197 the acceleration response spectrum results of the two groups of sea free field models are
 198 generally higher than those of the land model, and the response spectrum results of model 4
 199 are slightly higher than those of model 3. When the Kobe wave is input in the form of SV
 200 wave, there are two obvious peaks in the acceleration response spectrum, and the long period
 201 components of the acceleration response spectrum of the two groups of sea free field models
 202 are generally higher than that of the land model.

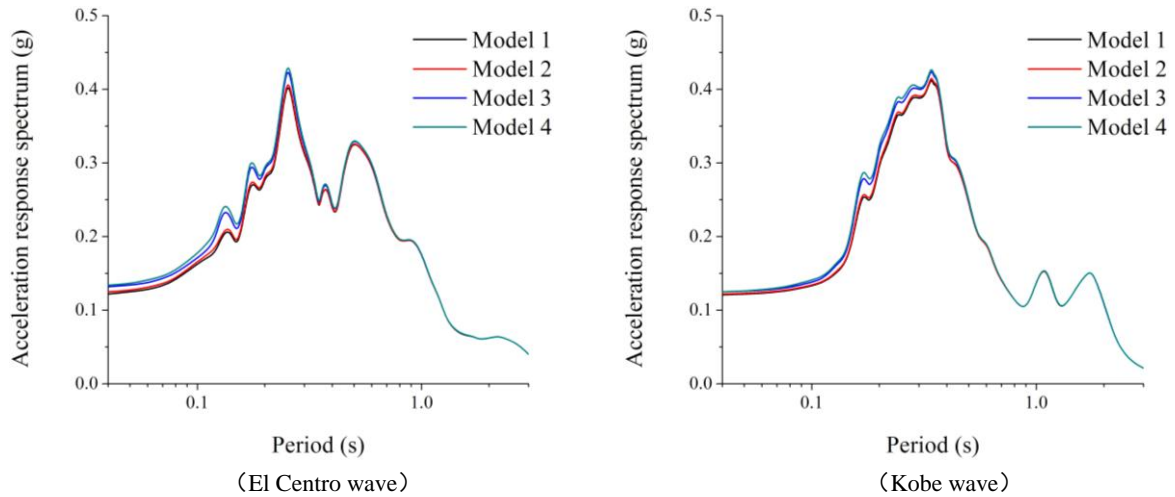
203



204

205

206 **Figure 3.** Acceleration response spectrum of point a of four free field models in the form of SV input

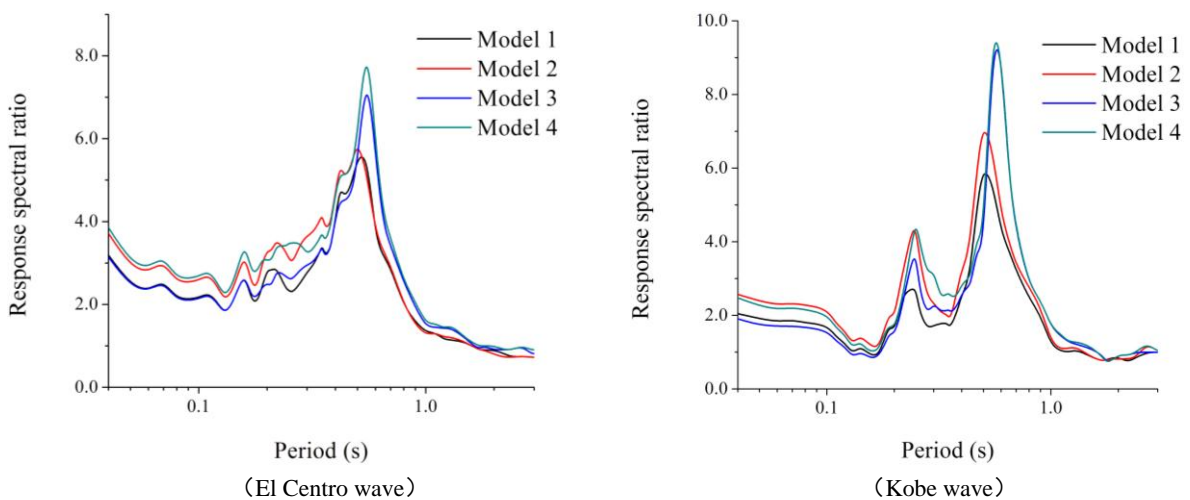


207
208

209 **Figure 4.** Acceleration response spectrum of point a of four free field models in the form of P-wave input
210

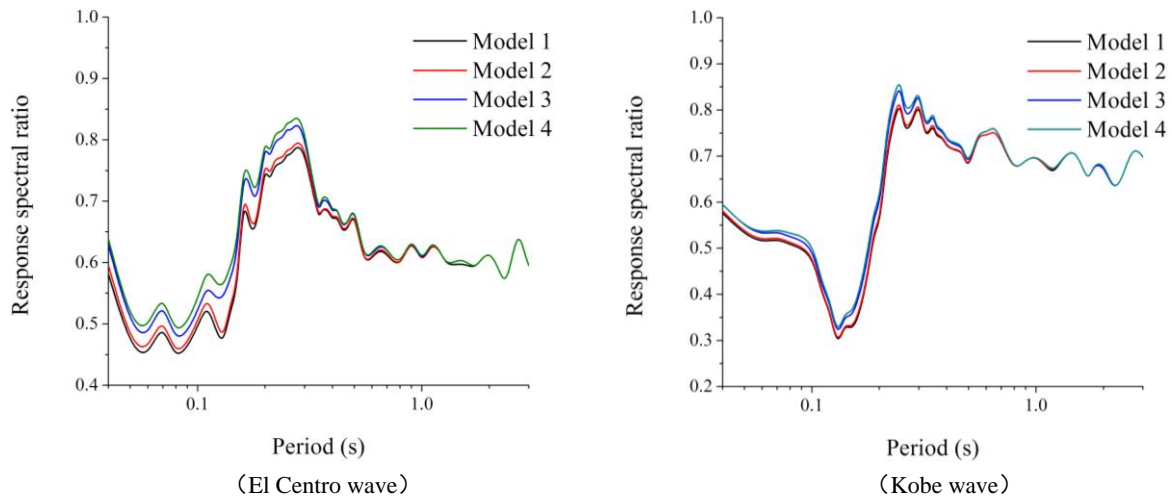
211 In order to investigate the amplification effect of the surface acceleration response
212 spectrum in each period, the result of the acceleration response spectrum is divided by the
213 base input response spectrum, and the result of the response spectral ratio is obtained, as
214 shown in figures 5 and 6, in which the input form of ground motion in figure 5 is SV wave,
215 and the input form of base ground motion in figure 6 is P wave.

216 According to figure 3 and figure 5, it can be found that the maximum value of reaction
217 spectral ratio appears at the periodic point of the maximum value of response spectrum for the
218 SV wave as input, and the amplification effect is very obvious, and the maximum
219 amplification factor is about 8 to 10. As the result of the input form of P wave, we find that
220 the period of the maximum acceleration response spectrum of figure 4 is inconsistent with
221 that of the maximum response spectral ratio of figure 6, and the result of the response spectral
222 ratio shows an undulating shape. Generally speaking, the surface response spectrum is not
223 magnified compared with the base response spectrum, and shows a shrinking result in each
224 period.
225



226
227

228 **Figure 5.** Response spectral ratio between the surface and the base input of SV wave form

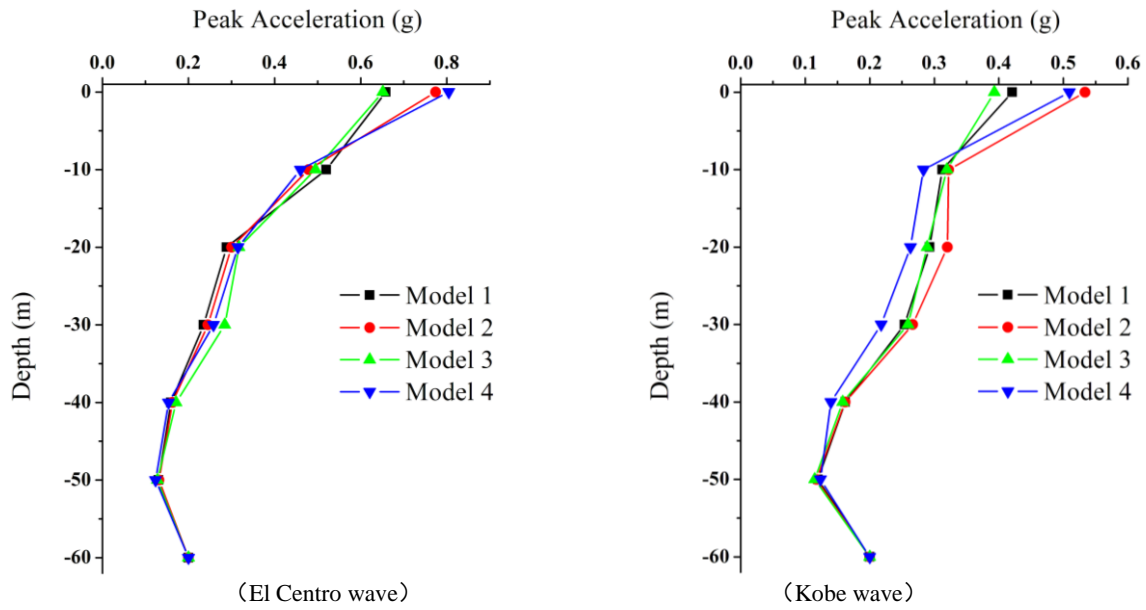


229
 230
 231 **Figure 6.** Response spectral ratio between the surface and the base input of P wave form

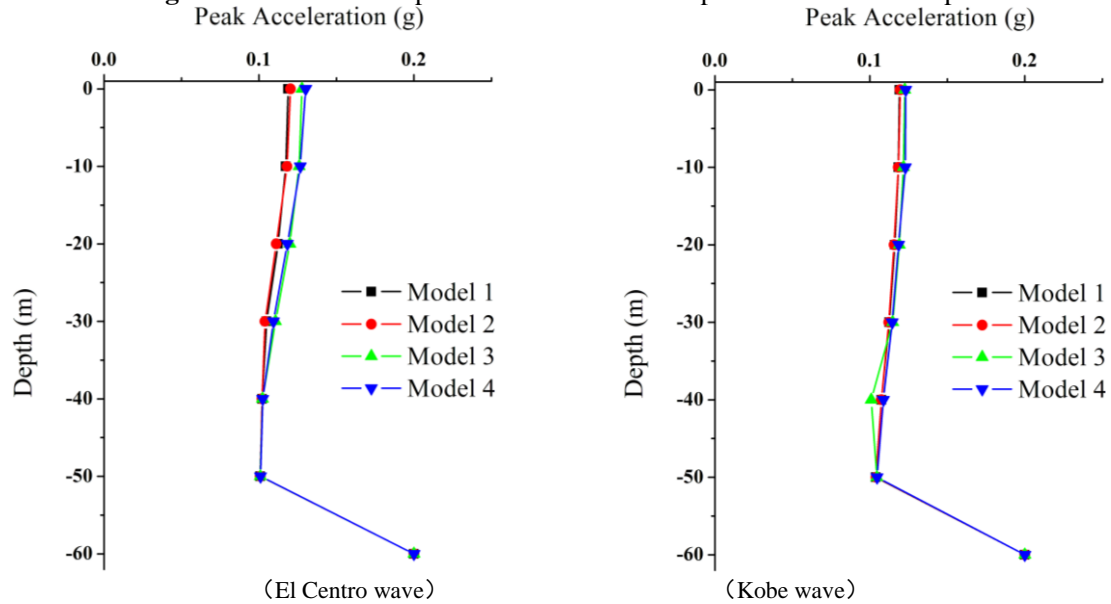
232 **4.4 Variation trend of amplification effect of ground motion along depth**

233 In order to analyze the propagation characteristics and attenuation law of seismic wave from
 234 the bottom of typical free field to the surface, in addition to monitoring point A of surface and
 235 seabed surface, monitoring calculation points are set every 10m for the above four groups of
 236 free field models, and the relationship curve of peak acceleration of four groups of free field
 237 models with the depth of soil layer is given. Figure 7 shows the results of SV wave input, and
 238 Figure 8 shows the results of P-wave input result. It can be seen from Figure 7 that the peak
 239 acceleration of the ground motion from the bottom to the surface decreases first and then
 240 increases, which shows that the ground motion changes at 50m underground and generally
 241 enlarges at the surface, as shown in Table 4. At the same time, Figure 7 also shows that the
 242 peak acceleration difference of four groups of free field models under the surface of 10 meters
 243 is small. Because there is no difference in the calculation parameters and physical and
 244 mechanical properties of the calculated model site soil, it shows that under the input condition
 245 of SV wave, the impact of overlying sea water and surface soft soil layer on the peak
 246 acceleration of ground motion under the surface is small.

247 For the case of P wave input, the difference of peak acceleration among the four groups of
 248 free field models is small, and the peak acceleration decreases first and then increases from
 249 the bottom to the surface, which shows that there is a change at 50m underground, and it
 250 shows a reduction effect on the surface as a whole. Similarly, under the condition of P-wave
 251 input, the effect of overlying sea water and soft soil layer on the peak acceleration of ground
 252 motion under the surface is unimportant.



253
254
255 **Figure 7.** Variation of peak acceleration with depth under SV wave input



256
257
258 **Figure 8.** Variation of peak acceleration with depth under P wave input

259 **5 conclusion**

260 In this paper, FLAC3D is used to construct four sets of typical free field calculation models.
261 Natural seismic waves of SV and P waves are used as the base input, and the finite difference
262 method is used to carry out two-dimensional seismic response analysis. Four sets of
263 calculation results of peak acceleration and acceleration response spectrum of typical free
264 field are obtained, and the following preliminary conclusions are summarized

265 (1) When the seismic wave is input in the form of SV wave, the surface soft soil can
266 amplify the peak acceleration of the surface and seabed surface, while the overlying sea water
267 can significantly reduce the ground motion. When the seismic wave is newly input as a base
268 in the form of P wave, the effect of overlying sea water and soft soil on the peak acceleration
269 of the surface and seabed surface is small and can be ignored.

270 (2) When El Centro wave is input as the base in the form of SV wave, the acceleration

271 response spectrum results of the two groups of sea free field models are generally higher than
272 those of the land model, and the response spectrum results of model 4 are slightly higher than
273 those of model 3. When the Kobe wave is input as the base in the form of SV wave, the long
274 period component of acceleration response spectrum of the two groups of sea free field
275 models is generally higher than that of the land model. Similar to the peak acceleration results,
276 when the seismic wave is input in the form of P wave, the difference between the four groups
277 of free field models is small.

278 (3) The peak acceleration decreases first and then increases from the bottom to the surface.
279 In addition to the results of the peak acceleration of the surface, the peak acceleration
280 difference between the layers of the underground obtained by each model is not obvious. For
281 the input of SV wave, the overlying seawater and soft soil layer have little effect on the peak
282 acceleration of ground motion below the surface, and show an amplification effect on the
283 whole at the surface. For the P-wave input, the difference of peak acceleration between the
284 underground layers is small, and the effect of reduction on the surface is overall.

285 In conclusion, through the comparative analysis of the two-dimensional seismic response
286 analysis results of four typical free field models, it shows that the overlying sea water and the
287 surface soft soil layer have certain influence on the ground motion, which is an important
288 factor that cannot be ignored in the actual engineering seismic design analysis and checking
289 calculation. Therefore, the conclusion of this paper is helpful to improve the understanding of
290 the dynamic characteristics of saturated soft soil and the amplification effect of site ground
291 motion, and has certain reference value for seismic design of sea area engineering.

292

293 *Data availability.* The data used to support the findings and results of this study are available
294 from the corresponding author upon request.

295

296 *Author contributions.* All authors (JL¹, JL², XS) contributed to this paper. JL¹ and JL²
297 discussed and wrote the original manuscript. JL² collected calculating data and established the
298 different models. JL¹ and XS ran the simulations, formal analysis, and data curation. JL¹ made
299 all the figures, and prepared the writing with contributions from all co-authors.

300

301 *Competing interests.* The authors declare that they have no conflict of interest.

302 *Financial support.* This research has been supported by the National Natural Science
303 Foundation of China (Grant No. 51408559), Guangxi Natural Science Foundation (Grant No.
304 2018GXNSFAA281183).

305 **References**

- 306 Bardet, J. P., Ichii, K., and Lin, C. H.: EERA, A computer program for equivalent-linear earthquake site
307 response analyses of layered soil deposits. Department of Civil Engineering, University of Southern
308 California, 2000.
- 309 Bardet, J. P. and Tobita, T.: NERA, A computer program for nonlinear earthquake site response analyses of
310 layered soil deposits. Department of Civil Engineering, University of Southern California, 2001.
- 311 Boore, D. M. and Smith, C. E.: Analysis of earthquake recordings obtained from the Seafloor Earthquake
312 Measurement System (SEMS) instruments deployed off the coast of southern California. Bulletin of the

313 Seismological Society of America, 89, 260-274.
314 <https://pdfs.semanticscholar.org/beed/fb15de864110a2a409a152ada4805cab027f.pdf>, 1999.

315 Celebi, M.: Topographical and geological amplification: case studies and engineering implications,
316 Structural Safety, 10, 199-217. [https://doi.org/10.1016/0167-4730\(91\)90015-2](https://doi.org/10.1016/0167-4730(91)90015-2), 1991.

317 Chen, B.: Characteristics of Offshore Ground Motions and Seismic Response Analysis of Sea-crossing
318 Bridges. Ph.D. Thesis, Dalian University of Technology, Dalian, 2016

319 Fan, S., Shi, Y., Liu, C., and Li, W.: Simulation of spatially varying seafloor ground motions with random
320 seawater layer and complex terrain, Soil Dynamics and Earthquake Engineering, 111, 110-118.
321 <https://doi.org/10.1016/j.soildyn.2018.02.007>, 2018.

322 Hashash, Y. M. A. and Park, D.: Non-linear one-dimensional seismic ground motion propagation in the
323 Mississippi embayment, Engineering Geology, 62, 185-206,
324 [https://doi.org/10.1016/S0013-7952\(01\)00061-8](https://doi.org/10.1016/S0013-7952(01)00061-8), 2001.

325 He, C., Wang, J., Zhang, C., and Jin, F.: Simulation of broadband seismic ground motions at dam canyons
326 by using a deterministic numerical approach, Soil Dynamics and Earthquake Engineering, 76, 136-144,
327 <https://doi.org/10.1016/j.soildyn.2014.12.004>, 2015.

328 Huang, Y., Ye, W., and Chen, Z.: Seismic response analysis of the deep saturated soil deposits in Shanghai.
329 Environmental geology, 56, 1163-1169. <http://doi.org/10.1007/s00254-008-1216-1>, 2009.

330 Idriss, I.M. and Sun, J. I.: SHAKE91: A computer for conducting equivalent linear seismic response
331 analyses of horizontally layered soil deposits. Department of Civil and Environmental Engineering,
332 University of California Davis; 1992.

333 Kubo, H., Nakamura, T., Suzuki, W., Dhakal, Y. P., Kimura, T., Kunugi, T., Takahashi, N., and Aoi, S.:
334 Ground-Motion Characteristics and Nonlinear Soil Response Observed by DONET1 Seafloor
335 Observation Network during the 2016 Southeast Off-Mie, Japan, Earthquake, Bulletin of the
336 Seismological Society of America, 109, 976-986, <http://doi.org/10.1785/0120170296>, 2019.

337 Lan, J., Liu, H., and Lyu, Y.: Dynamic nonlinear parameters of soil in the Bohai Sea and their rationality,
338 Journal of Harbin Engineering University, 2012, 33, 1079-1085,
339 <http://doi.org/10.3969/j.issn.1007-7043.201202036>, 2019.

340 Meng, J.: Earthquake ground motion simulation with frequency-dependent soil properties, Soil Dynamics
341 and Earthquake Engineering, 27, 234-241. <https://doi.org/10.1016/j.soildyn.2006.07.002>, 2007.

342 Nakamura, T., Nakano, M., Hayashimoto, N., Takahashi, N., Takenaka, H., Okamoto, T., Araki, E., and
343 Kaneda, Y.: Anomalous large seismic amplifications in the seafloor area off the Kii peninsula, Mar
344 Geophys. Res., 35, 255-270, <http://doi.org/10.1007/s11001-014-9211-2>, 2014.

345 Petukhin, A., Iwata, T., and Kagawa, T.: Study on the effect of the oceanic water layer on strong ground
346 motion simulations, Earth, Planets and Space, 62, 621-630, <https://doi.org/10.5047/eps.2010.07.014>,
347 2010.

348 Streeter, V. L., Wylie, E. B., and Richart, F. E.: Soil motion computation by characteristic method, Journal
349 of the Geotechnical Engineering Division, 100, 247-263, 1974.

350 Wang, S. and Hao, H. Effects of random variations of soil properties on site amplification of seismic
351 ground motions. Soil Dynamics and Earthquake Engineering, 22, 551-564,
352 [https://doi.org/10.1016/S0267-7261\(02\)00038-6](https://doi.org/10.1016/S0267-7261(02)00038-6), 2002.

353 Wang, Z., Carpenter, N. S., and Woolery, E. W.: Horizontal-to-vertical spectral ratio of S-waves and
354 SH-wave transfer functions at the vertical seismic and strong-motion arrays in the central United States,
355 Journal of Applied Geophysics, 162, 64-71, <https://doi.org/10.1016/j.jappgeo.2018.10.017>, 2019.

356 Yang, J.: Saturation effects on horizontal and vertical motions in a layered soil-bedrock system due to

357 inclined SV waves, Soil Dynamics and Earthquake Engineering, 21, 527–536.
358 [https://doi.org/10.1016/S0267-7261\(01\)00015-X](https://doi.org/10.1016/S0267-7261(01)00015-X), 2001.

359 Yang, J. and Sato, T.: Influence of water saturation on horizontal and vertical motion at a porous soil
360 interface induced by incident SV wave, Soil Dynamics and Earthquake Engineering, 19, 339–346.
361 [https://doi.org/10.1016/S0267-7261\(00\)00023-3](https://doi.org/10.1016/S0267-7261(00)00023-3), 2000.

362 Zhang, D., Xie, W., and Pandey, M. D.: Synthesis of spatially correlated ground motions at varying sites
363 based on vector-valued seismic hazard deaggregation, Soil Dynamics and Earthquake Engineering, 41,
364 1–13. <https://doi.org/10.1016/j.soildyn.2012.04.009>, 2012.

365 Zhang, K., Zhao, C., and Li, W.: Study of the seismic response of the seafloor ground containing soft soil,
366 Rock and Soil Mechanics, 40, 2456-2468, <https://doi.org/10.16285/j.rsm.2018.1165>, 2019.